

A COMPARATIVE ANALYSIS OF ENDMEMBER EXTRACTION ALGORITHMS USING AVIRIS HYPERSPECTRAL IMAGERY

Antonio Plaza, Pablo Martínez, Rosa M. Perez, Javier Plaza¹

1. Introduction

Spectral unmixing techniques are widely used for hyperspectral data analysis and quantification. Many novel applications have been developed from the unmixing point of view, including surface constituent identification for land use mapping, disaster assessment, geology, biological process analysis and change detection (Keshava and Mustard, 2002). All existing unmixing approaches require a previous step where the spectral signatures of ground constituents (endmembers) are identified (Kruse, 1998; Boardman et al., 1995), and then a mixture model is used to estimate the abundance fractions of these signatures by expressing individual pixels as a linear or non-linear combination of endmembers (Bateson et al., 2000). The accuracy of the quantification depends strongly on how accurate endmembers are identified in the first step.

Several different strategies have been proposed to evaluate the quality of selected endmembers for spectral unmixing. The simplest approach has been direct comparison to reference signatures contained in a spectral library of ground measurements (Winter, 2000; Sweet et al., 2000). Another alternative has been focused on analyzing the abundance of endmembers in the scene, which is usually expressed as a series of greyscale images where the grey level value at each pixel represents a combined amount of the abundance of endmembers contained in the pixel. Then, the quality of a set of endmembers may be evaluated by comparing their associated abundance fractions to reference abundance planes, either by visual comparison (Winter, 2000; Kneubuehler et al., 1998) or, more reliably, by statistical measures like the average root mean square error (RMSE) (García and Ustin, 2001) or the Pearson correlation coefficient (Maselli, 1998).

The previous approaches are possible when ground truth data is available and contains information about the abundance of materials in each pixel of the scene. Nevertheless, it should be noted that the obtention of reliable ground truth is difficult, expensive and very time-consuming, a fact that has traditionally prevented the existence of reliable ground measurements for a large number of datasets.

Some approaches have been previously considered in order to assess endmember extraction accuracy when no ground truth information is available. Most of them are based on a reconstruction process of the original hyperspectral image, using the set of extracted endmembers and their estimated abundance maps, according to linear spectral mixture model definitions. The generated image may be compared to the original one by several statistical measures (Bowles et al., 2000).

However, in many reconstruction-oriented approaches, an important question arises: the number of endmember vectors required to accurately approximate or regenerate the pixels of the original image. In order to answer this question, several authors have proposed to consider multiple sets of endmembers simultaneously for spectral unmixing (Roberts et al., 1998, Okin et al., 1998, Bateson et al., 2000). Following this idea, some studies have demonstrated that models based on three endmembers generally provide satisfactory results although, in some applications, models based on four and more endmembers improve considerably the results found using only three endmembers (Segl et al., 2000; Garcia and Ustin, 2001). In general terms, it is expected that the quality of the reconstruction process would improve as the number of reference signatures used increases, even though mixed pixels are used in the reconstruction process. Nevertheless, the goal should be the identification of a reduced subset of pure spectral signatures which are able to provide a reconstruction which is similar enough (i.e., under a certain error tolerance threshold) to the original image.

Although several comparative efforts have been proposed in recent years, no unified criterion has been accepted for rigorous and impartial comparison of endmember extraction algorithms. The importance of this issue cannot be understated since, without effective evaluation criteria, the performance of any new algorithm cannot be substantiated. In this paper, we take a first step by conducting a comparative study of performance analysis among several existing endmember extraction algorithms, including the Pixel Purity Index (Boardman et al., 1995), the N-FINDR algorithm (Winter, 2000) and our custom-designed method Automated Morphological Endmember Extraction, AMEE (Plaza et al., 2002; Plaza et al., 2001a; Plaza et al., 2001b). A novel comparative framework is introduced, allowing detailed quantitative assessment of endmember

¹ Neural Networks and Signal Processing Group (GRNPS), Computer Science Department, University of Extremadura.
Avda. de la Universidad s/n, 10.071 Cáceres, SPAIN. E-mail: aplaza@unex.es, pablomar@unex.es, rosapere@unex.es.

extraction accuracy. The significance of these experimental results is to offer a performance evaluation of endmember detection algorithms in a rigorous fashion so that each algorithm is fairly compared to others on the same common context. Several different situations are considered in the above framework, regarding the availability or not of ground truth data and the intrinsic characteristics of such information.

The paper is organized as follows. Section 2 defines an objective framework for evaluation of endmember extraction and subsequent classification accuracy. Section 3 presents a comparative performance analysis for the above-mentioned algorithms, and section 4 concludes with some remarks.

2. Comparative framework for evaluation of endmember extraction algorithms

In this section, a schema to evaluate endmember extraction algorithms is proposed. The framework has into account the following situations:

- 1) Ground truth (GT) is available in the form of a spectral library of constituent signatures.
- 2) GT contains the abundance of endmember materials for each pixel of the scene.
- 3) GT is not available.

We proceed to describe the evaluation approach to validate extracted endmembers in each situation.

2.1. Evaluation by Comparison to GT Spectral Signatures

Before addressing the metrics used to evaluate endmember quality in this case, the following definitions are introduced:

N	Total number of pixels in the original hyperspectral image.
$\Gamma_E = \{E_i\}_{i=1}^K$	Set containing X endmembers extracted from the hyperspectral image.
$E_i = (E_i(\lambda_1), E_i(\lambda_2), \dots, E_i(\lambda_S))^T$	A particular endmember of Γ_E .
$\Gamma_R = \{R_i\}_{i=1}^K$	Set containing Y GT signatures.
$R_i = (R_i(\lambda_1), R_i(\lambda_2), \dots, R_i(\lambda_S))^T$	A particular GT signature of Γ_R .

A correlation matrix of spectral angle distances (SAM matrix) is used to perform the comparison in this situation. Figure 1 shows an example of the construction of a SAM matrix between extracted endmembers and GT signatures. In this representation, we denote $SAM_{nm} = SAM(E_n, R_m)$, where SAM refers to the cosine of the spectral angle.

		Endmember signatures			
		E_1	E_2	...	E_X
GT signatures	R_1	SAM_{11}	SAM_{21}	...	SAM_{X1}
	R_2	SAM_{12}	SAM_{22}	...	SAM_{X2}
	\vdots	\vdots	\vdots		\vdots
	R_Y	SAM_{1Y}	SAM_{2Y}	...	SAM_{XY}

Figure 1. SAM matrix between extracted and reference signatures.

2.2. Evaluation by Comparison to GT Abundance Planes

This schema is based on the assumption that each evaluated endmember E_i has an associated GT signature R_i . Both E_i and R_i have associated abundance maps, $G(E_i)$ and $G(R_i)$, which respectively contain the fractional abundance of the spectral signature in the pixels of the original image. Before addressing the quality measures used in this situation, the following definitions are introduced:

$I = \{P_j\}_{j=1}^N$	Original hyperspectral image expressed as a set of N hyperspectral pixels.
$P_j = (P_j(\lambda_1), P_j(\lambda_2), \dots, P_j(\lambda_S))^T$	A particular pixel of the image.
$\Phi_j(E_i)$	Fractional abundance of endmember material E_i at pixel P_j of the original image.
$\Phi_j(R_i)$	Fractional abundance of reference material R_i at pixel P_j of the original image.
$G(E_i) = \{\Phi_j(E_i)\}_{j=1}^N$	Greyscale abundance map of endmember E_i .
$G(R_i) = \{\Phi_j(R_i)\}_{j=1}^N$	Greyscale abundance map of reference signature R_i .

Each E_i, R_i pair is compared at a pixel level by calculating the root mean square error between their associated abundance maps using the following expression.

$$\text{RMSE}_I\{G(E_i), G(R_i)\} = \sqrt{\sum_{i=1}^N (\Phi_j(E_i) - \Phi_j(R_i))^2}$$

2.3. Evaluation when ground truth is not available

The approach that we present to compare endmembers when no ground truth information is available is only applicable when the linear mixture model is suitable to perform the analysis and classification of the scene. The linear approach has been demonstrated in numerous applications to be a useful technique for interpreting the variability in remote sensing data. Nevertheless, it is only strictly valid for the situation where the endmembers are arranged in discrete, segregated patches on the surface (Keshava and Mustard, 2002). This condition is hardly met in nature, and many constituents of interest for earth science investigations exist in soils, or at smaller scales, in intimate association with one another. In this work, we rely on the linear model as an initial attempt to validate our framework, but we are aware that the use of this model may introduce errors in the comparison.

Once this initial statement has been made, we proceed to describe our comparative framework in this situation. Using the previously defined notations, a particular pixel P_j in the original hyperspectral image can be approximated by the following expression:

$$P_j \approx P_j' = \sum_{i=1}^p \Phi_j(E_i) \cdot E_i,$$

where $\Phi_j(E_i)$ denotes the abundance fraction of endmember material E_i at pixel P_j . The accuracy of the approximation in (12) for a single P_j using a set of endmembers Γ_E can be quantified by the root mean square error:

$$\text{RMSE}_I(\Gamma_E) = \sqrt{\sum_{i=1}^N \left(P_j - \sum_{i=1}^p \Phi_j(E_i) \cdot E_i \right)^2}$$

In order to study the capacity of extracted endmembers to provide an accurate reconstruction of the original image, we consider a variable number of endmembers to perform the reconstruction. Our goal is to analyze the optimum number of endmembers needed to reconstruct the original image, and also to evaluate the accuracy of such reconstruction. In order to achieve the previously addressed objectives, the following algorithm is used.

Step 1) Set a tolerance threshold T .

Step 2) Calculate the abundance of each endmember E_i in image I : $\forall E_i, G(E_i) = \{\Phi_j(E_i)\}_{j=1}^N$.

Step 3) Order the endmembers in set Γ_E according to their total abundance in the original image. The total abundance of

$$\text{endmember } E_i \text{ in image } I \text{ is calculated as: } \sum_{j=1}^N \Phi_j(E_i).$$

Step 4) Construct a new set Γ_N which contains the three most abundant endmembers of Γ_E , and remove such endmembers from Γ_E .

Step 5) If $\text{RMSE}_I(\Gamma_N) < T$ then stop (a satisfactory reconstruction is achieved).

Step 6) Remove the most abundant endmember in Γ_E and incorporate it to Γ_N .

Step 7) Repeat from step 5 until $\Gamma_E = \emptyset$ (in this case, no satisfactory reconstruction was possible).

3. Results and discussion

The following endmember extraction methods: PPI, N-FINDR and AMEE were applied to hyperspectral datasets obtained by the NASA/JPL-AVIRIS imaging spectrometer (Green et al., 1988). Also, a preliminary evaluation of the above methods was performed using data from the DAIS 7915 and ROSIS imaging spectrometers from DLR (Müller et al., 2001).

- The AVIRIS hyperspectral dataset corresponds to the well-known mining region of Cuprite in Nevada. This area is well-understood mineralogically and has reliable ground truth in several forms (Clark et al., 1993; Swayze, 1997). This fact has made this region a standard test site for comparison of classification algorithms, since not many scenes with such quality ground truth measurements are available for public use. The Cuprite scene we have selected for this work was acquired in 1995, and has been reduced to 50 bands in the 2-2.5 μm region.
- The DAIS 7915 and ROSIS hyperspectral datasets were acquired near the town of Cáceres, Spain, in 2001. These data are a good example of Dehesa agroecosystems, typical of the south-western part of Spain and mainly formed by cork-oak trees, pasture and bare soils (semi-arid environment). Our knowledge of the field, obtained after several ground campaigns, make these dataset suitable to test algorithm accuracy. Next, we proceed to describe the experiments performed over these datasets.

3.1. Experiments with AVIRIS hyperspectral dataset

a) First experiment: comparison of the spectral shape

In order to perform this experiment we have selected a set of ground spectral signatures contained in the USGS Digital Spectral Library splib04 (available at <http://speclab.cr.usgs.gov/spectral.lib04/spectral-lib04.html>) as ground truth references for the comparison. In particular, we have used the AVIRIS-convolved version of this library (<http://speclab.cr.usgs.gov/spectral.lib04/lib04-AVIRIS.html>).

Figure 2 shows a plot of the GT signatures from the USGS spectral library and the endmembers extracted by PPI, N-FINDR and AMEE algorithms. PPI endmembers were obtained and made public by Research Systems. N-FINDR endmembers were obtained by Dr. Michael E. Winter, author of the algorithm. Finally, AMEE endmembers were extracted by our research group. The USGS spectra are labeled in the plot with their correspondent names in the library. PPI endmembers were labeled with the names that appear in the plot, while N-FINDR and AMEE spectra are not labeled. The colors used in figure 2 have been selected so that the similar spectral signatures can be visually matched. It is appreciated in figure 2 that there are some differences in the absolute value of the reflectances and spectral shape that are likely due to atmospheric transmission effects. In order to avoid these effects, we use the SAM distance measure, which is invariant to illumination details.

Tables I, II and III respectively show the confusion matrices of spectral angle distances between USGS GT signatures and the endmembers extracted by PPI, N-FINDR and AMEE. Table IV shows the number of correctly detected endmembers, redundant endmembers, missed GT signatures and mean error for the considered endmember extraction algorithms using three different similarity threshold values. In order to understand the results shown in this table it should be noted that perfect performance for a certain algorithm would be correct detection of all endmembers and no missed GT signatures or redundant endmembers, independently of the similarity threshold considered. The results shown in table IV reveal that, when a strong similarity threshold is imposed, the three tested algorithms perform similarly. When the similarity constraint is relaxed, AMEE performs better than the other approaches, detecting all endmember signatures and producing only 2

redundant endmembers, which correspond to the ones labeled as AMEE_ENDMEMBER_8 and AMEE_ENDMEMBER_9 in figure 2. It should be noted that AMEE_ENDMEMBER_9 is a typical shade endmember, while AMEE_ENDMEMBER_8 is associated to the brightest parts of the Silica mineral (a similar endmember is also detected by the PPI algorithm).

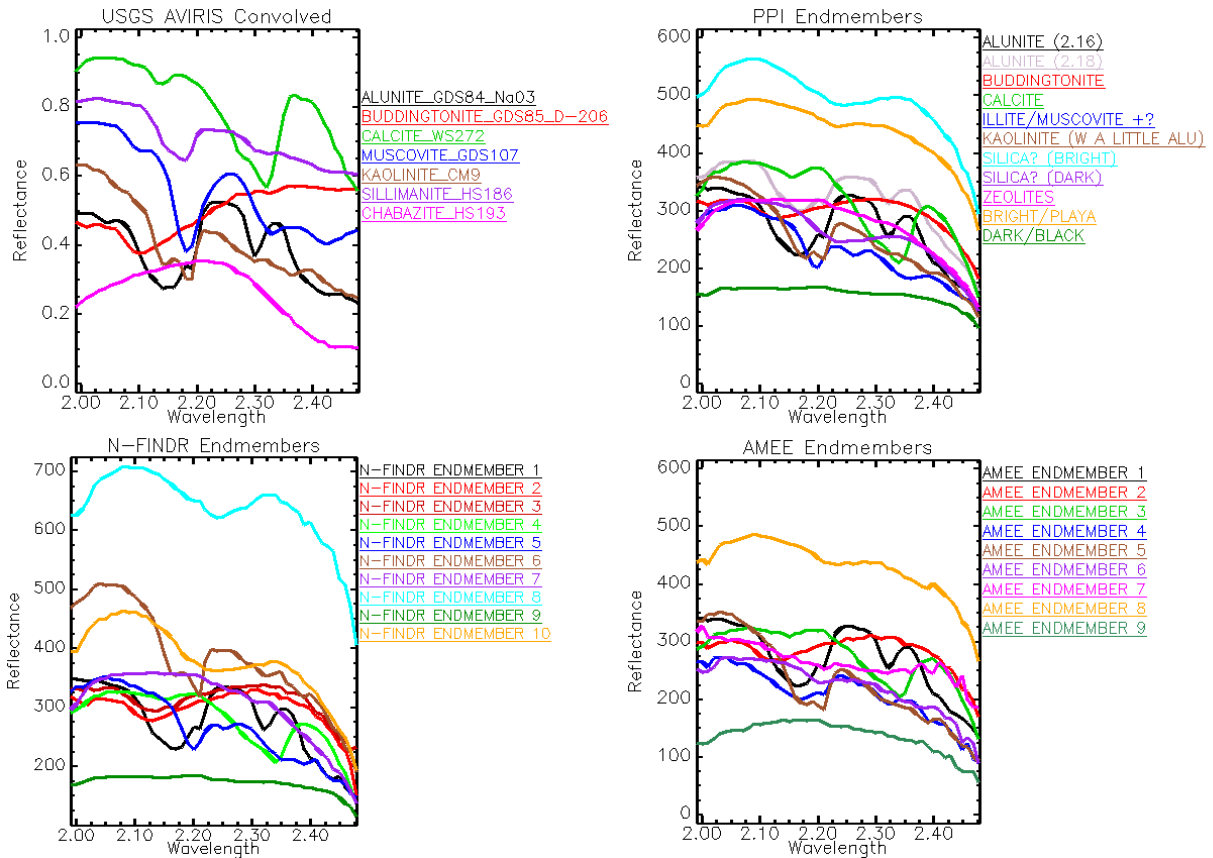


Figure 2. Clockwise, reference GT signatures extracted from AVIRIS-convolved USGS Digital Spectral Library and endmembers extracted for the Cuprite dataset by PPI, N-FINDR and AMEE methodologies.

Table I. Confusion matrix of spectral angle distances between endmembers extracted by PPI and USGS GT references.

	PPI:										
USGS:	E1	E2	E3	E4	E5	E6	E7	E8	E9	E10	E11
Alunite	0.119	0.155	0.208	0.178	0.265	0.207	0.238	0.208	0.216	0.230	0.206
Buddingtonite	0.286	0.269	0.228	0.188	0.319	0.208	0.343	0.359	0.231	0.302	0.287
Calcite	0.136	0.104	0.085	0.093	0.149	0.088	0.140	0.157	0.084	0.124	0.132
Muscovite	0.256	0.229	0.232	0.263	0.234	0.241	0.238	0.268	0.247	0.223	0.167
Kaolinite	0.164	0.178	0.223	0.233	0.208	0.236	0.139	0.093	0.218	0.189	0.226
Sillimanite	0.151	0.149	0.181	0.199	0.186	0.197	0.103	0.090	0.177	0.161	0.194
Chabazite	0.194	0.151	0.112	0.142	0.095	0.114	0.148	0.183	0.103	0.117	0.144

Table II. Confusion matrix of spectral angle distances between endmembers extracted by N-FINDR and USGS GT references.

	N-FINDR:									
USGS:	E1	E2	E3	E4	E5	E6	E7	E8	E9	E10
Alunite	0.211	0.233	0.119	0.241	0.182	0.208	0.180	0.225	0.205	0.282
Buddingtonite	0.192	0.338	0.283	0.283	0.178	0.300	0.167	0.279	0.320	0.247
Calcite	0.085	0.137	0.132	0.121	0.113	0.143	0.092	0.105	0.121	0.175
Muscovite	0.255	0.235	0.256	0.227	0.276	0.146	0.279	0.234	0.257	0.319
Kaolinite	0.243	0.141	0.164	0.210	0.249	0.226	0.240	0.195	0.127	0.284
Sillimanite	0.201	0.102	0.149	0.181	0.219	0.196	0.205	0.159	0.098	0.251
Chabazite	0.117	0.152	0.191	0.083	0.159	0.154	0.148	0.109	0.147	0.179

Table III. Confusion matrix of spectral angle distances between endmembers extracted by AMEE and USGS GT references.

	AMEE:								
USGS:	E1	E2	E3	E4	E5	E6	E7	E8	E9
Alunite	0.119	0.213	0.179	0.243	0.232	0.162	0.248	0.216	0.213
Buddingtonite	0.286	0.227	0.125	0.289	0.297	0.316	0.415	0.311	0.226
Calcite	0.194	0.109	0.153	0.087	0.173	0.158	0.230	0.136	0.084
Muscovite	0.151	0.178	0.212	0.184	0.234	0.127	0.122	0.155	0.147
Kaolinite	0.164	0.221	0.244	0.211	0.268	0.136	0.100	0.185	0.183
Sillimanite	0.136	0.081	0.145	0.127	0.169	0.128	0.213	0.129	0.058
Chabazite	0.256	0.237	0.270	0.225	0.143	0.221	0.298	0.194	0.284

Table IV. Mean error, number of matched endmembers, redundant endmembers and missed GT signatures for each method using three different tolerance threshold errors.

	T = 0.10					T = 0.15				T = 0.20			
Method:	NE	MEr	MEn	MG	RE	MEr	MEn	MG	RE	MEr	MEn	MG	RE
PPI	11	0.090	3	4	8	0.105	5	2	6	0.115	6	2	5
N-FINDR	10	0.091	3	4	7	0.106	5	2	5	0.110	6	1	4
AMEE	9	0.081	3	4	6	0.101	7	0	2	0.108	7	0	2

NE – Number of extracted endmembers MEr – Mean error MEn – Number of matched endmembers
 MG – Number of missed GT signatures T – Tolerance threshold RE – Number of redundant endmembers

b) Second experiment: comparison of fractional abundance maps

In this experiment, we have focused on comparing the fractional abundance maps derived from the endmembers shown in figure 2. Abundance maps of GT USGS signatures, obtained using Fully Constrained Linear Spectral Unmixing (FCLSU) are used as ground truth information. The experiment presented in the previous subsection revealed that five USGS signatures are easily detected by all the studied endmember extraction algorithms: Alunite, Buddingtonite, Calcite, Kaolinite and Muscovite. Following this result, we have calculated the abundance planes of the endmembers obtained by PPI, N-FINDR and AMEE for the previously addressed minerals, using a FCLSU approach.

Table V. Root Mean Square Error (RMSE) obtained by comparing FCLSU fractional abundances of selected USGS GT signatures to FCLSU abundance maps of correspondent extracted endmembers. The average RMSE for the signatures considered is also addressed.

USGS-derived Abundance Map	PPI Map	N-FINDR Map	AMEE Map
Alunite	0.071	0.072	0.070
Buddingtonite	0.170	0.150	0.157
Calcite	0.011	0.023	0.020
Kaolinite	0.048	0.089	0.009
Muscovite	0.042	0.045	0.063
Average	0.068	0.075	0.064

A detailed quantitative study of the quality of derived abundance planes has been carried out by calculating the RMSE between pairs of correspondent abundance maps. The results obtained are shown in Table V, which also addresses the mean error for each method. This table reveals that the similarity between the obtained abundance maps is very high in general, although the performance is slightly different depending on the mineral considered. AMEE algorithm obtains the best result for the Alunite and Kaolinite materials, while PPI is the most successful algorithm with the Calcite and Muscovite and N-FINDR is the best approach with Buddingtonite.

c) Third experiment: reconstruction of the original image

In this experiments we test the accuracy of the considered approaches to provide a reconstruction of the original image. Table VI shows a comparison of the RMSE errors obtained by the considered approaches, using the algorithm shown in section 2.3.

Table VI. RMSE errors obtained by the proposed endmember extraction algorithms in the reconstruction of AVIRIS Cuprite dataset.

	Number of endmembers used in the reconstruction (ordered by total abundance):								
	3	4	5	6	7	8	9	10	11
PPI	0.197	0.168	0.144	0.123	0.100	0.075	0.060	0.045	0.032
N-FINDR	0.197	0.115	0.098	0.086	0.073	0.063	0.054	0.049	
AMEE	0.174	0.128	0.102	0.074	0.055	0.046	0.042		

From this table, PPI is the most accurate method when all extracted endmembers are used in the reconstruction (3.2% error versus 4.9% of N-FINDR and 4.2% of AMEE). Nevertheless, when the number of endmembers used in the reconstruction is reduced, both N-FINDR and AMEE outperform PPI. For instance, if 7 endmembers are used for the reconstruction, the use of PPI results in a 10% error, while N-FINDR reduces the error to 7.3% and AMEE results in just a 5.5% error, which is a significant improvement over PPI. Further experiments are required to validate the previously addressed results using additional datasets and different conditions.

3.2. Experiments with DAIS 7915 and ROSIS hyperspectral datasets

In this section, we address some preliminary results obtained after applying our AMEE algorithm to DAIS 7915 and ROSIS hyperspectral datasets, obtained over the town of Cáceres, Spain, in July 2001. These results are showed just for illustrative (not comparative) purposes. In the future, the development of several ground campaigns will allow us to make these images, along with quality ground measurements, available to the scientific community dedicated to hyperspectral data analysis as test images to validate endmember extraction and classification algorithms. Figures 3 and 4 show extracted endmembers and corresponding abundance maps for DAIS 7915 and ROSIS imagery, respectively.

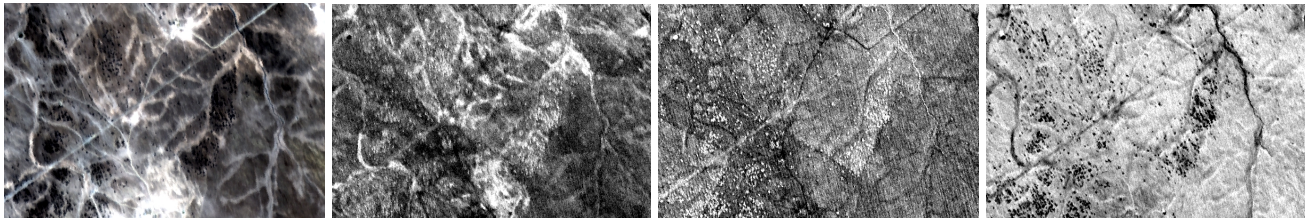
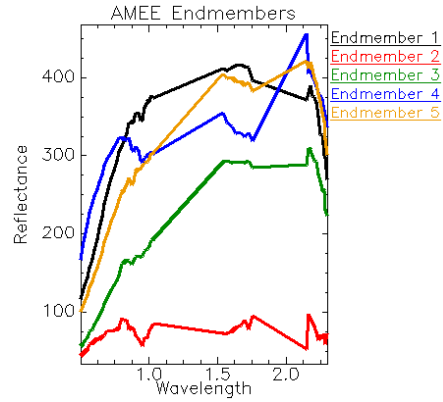


Figure 3. Preliminary endmember extraction results of AMEE algorithm applied to DAIS 7915 hyperspectral data. Top: extracted endmembers. Bottom, left to right: original image; abundance map for Endmember_1 (soil-pasture); abundance map for Endmember_2 (cork-oak trees); abundance map for Endmember_3 (shadow).

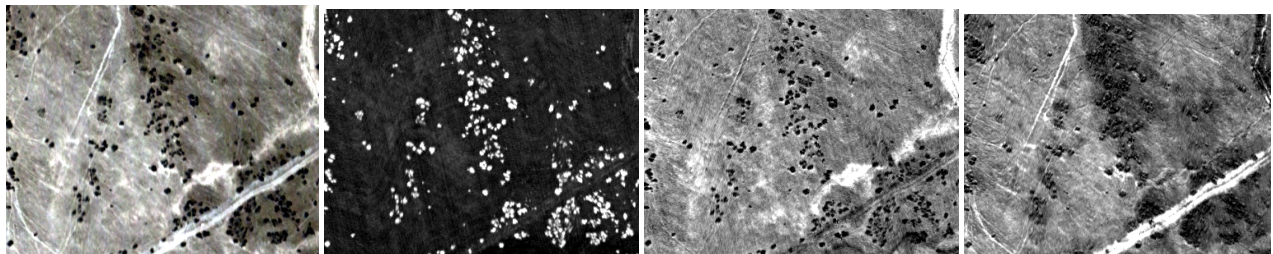
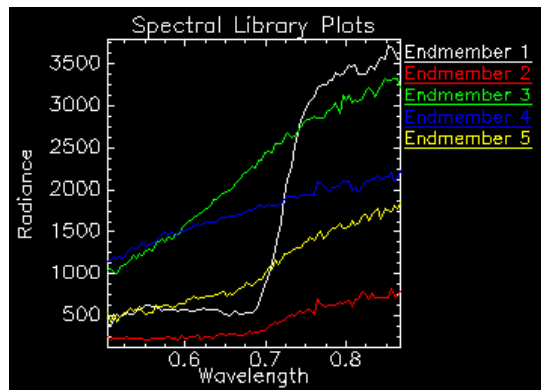


Figure 4. Preliminary endmember extraction results of AMEE algorithm applied to ROSIS hyperspectral data. Top: extracted endmembers. Bottom, left to right: original image; abundance map for Endmember_1 (cork-oak trees); abundance map for Endmember_2 (soil); abundance map for Endmember_3 (pasture).

4. Conclusions and future lines

Many endmember extraction algorithms have been proposed in the literature over the last decade. Comparison of these approaches has been a challenging task due to a lack of rigorous criteria to substantiate any new algorithm. Another difficulty arises from the fact that there is no standardized data to perform the comparison. In this paper, we have conducted a first attempt to impartially evaluate the accuracy of several well-known endmember extraction algorithms. The study focuses on two hyperspectral datasets: the famous AVIRIS dataset of the Cuprite mining region in Nevada (a well-understood mineralogically region which has been extensively mapped and truthed) and a DAIS 7915 dataset containing a typical Spanish Dehesa environment (pasture and cork-oak trees).

Comparison of endmembers has been carried out from several points of view. Firstly, the problem was tackled under the assumption that reliable ground truth information is available. In this sense, we performed a simple preliminary experiment based on comparing the spectral shape of extracted endmembers to available reference signatures. A further attempt from the perspective of a mixed pixel classification problem was also conducted by comparing abundance planes of endmember constituents to reference maps. Finally, a new schema to compare algorithms when no ground truth measurements are available was presented and discussed. Since reliable ground truth is generally expensive and difficult to obtain, we believe this approach may be of interest to the community.

Despite our effort to conduct comprehensive, impartial and rigorous comparative analysis of various algorithms, completion is not claimed. In particular, the number of algorithms compared in this work is limited to three methods. Also, the number of comparative measures is reduced to linear distances. Plausible future research should include a comparative analysis of linear and non linear distances, as well as comparative measures that include second order statistics.

Acknowledgments

The authors would like to acknowledge Robert O. Green and Roger Clark for their comments on this comparative effort. Also, the contribution of Michael and Ed Winter, who provided results and an evaluation version of the N-FINDR method, is gratefully acknowledged. Finally, Antonio Plaza would like to personally thank Robert O. Green and the whole AVIRIS team for their guidance, support and warm hospitality during his research visit to JPL.

References

- Bateson, C.A., Asner, G.P., Wessman, C.A., "Endmember Bundles: A New Approach to Incorporating Endmember Variability into Spectral Mixture Analysis," *IEEE Transactions on Geoscience and Remote Sensing*, vol. 38 issue 2 part: 2, pp. 1083-1094, March 2000.
- Boardman, J.W., Kruse, F.A. & Green, R.O., "Mapping Target Signatures via Partial Unmixing of AVIRIS Data," *Summaries of the V JPL Airborne Earth Science Workshop*, 1995.
- Bowles, J., Gillis, D., Palmadesso, P., "New improvements in the ORASIS algorithm," *Aerospace Conference Proceedings*, vol. 3, pp. 293-298, 2000.
- Clark, R. N., Swayze, G. A., Gallagher, A., King, T. V. V., and Calvin, W. M., "The U. S. Geological Survey Digital Spectral Library: Version 1: 0.2 to 3.0 m," *U. S. Geological Survey, Open File Report 93-592*, 1340 p, 1993.
- Garcia, M., Ustin, S.L., "Detection of interannual vegetation responses to climatic variability using AVIRIS data in a coastal savanna in California," *IEEE Transactions on Geoscience and Remote Sensing*, vol. 39, pp. 1480-1490, 2001.
- Green, R.O. et al., "Imaging Spectroscopy and the Airborne Visible/Infrared Imaging Spectrometer (AVIRIS)," *Remote Sensing of Environment*, vol. 65, pp. 227-248, 1998.
- Keshava, N., Mustard, J.F., "Spectral unmixing," *IEEE Signal Processing Magazine*, vol. 19, pp. 44-57, 2002.
- Kneubuehler, M., Schaepman, M.E., Kellenberger, T.W., "Comparison of different approaches of selecting endmembers to classify agricultural land by means of hyperspectral data (DAIS7915)," *Proceedings International Geoscience and Remote Sensing Symposium*, vol. 2, pp. 888-890, 1998.
- Kruse, F.A., "Spectral Identification of Image Endmembers Determined from AVIRIS Data," *Summaries of the VII JPL Airborne Earth Science Workshop*, 1998.
- Maselli, F., "Multiclass spectral decomposition of remotely sensed scenes by selective pixel unmixing," *IEEE Transactions on Geoscience and Remote Sensing*, vol. 36, pp. 1809-1820, 1998.

- Müller, A., Hausold, A., Strobl, P., "HySens – DAIS / ROSIS Imaging Spectrometers at DLR," *Proc. SPIE Image and Signal Processing for Remote Sensing VII*, Toulouse, France, 2001.
- Okin, G.S, Roberts, D.A., Murray, B., "Multiple Endmember Spectral Mixture Analysis: Application to an Arid/Semi-arid Landscape," *Summaries of the IX JPL Airborne Earth Science Workshop*, 1998.
- Plaza, A., Martínez, P., Perez, R.M., "Spatial/Spectral Endmember Extraction by Multidimensional Morphological Operations," *IEEE Transactions on Geoscience and Remote Sensing*, vol. 40, no. 9, Sept. 2002.
- Plaza, A., Martínez, P., Gualtieri, J.A., Pérez, R.M., "Spatial/Spectral Endmember Extraction from AVIRIS Hyperspectral Data Using Mathematical Morphology," *Summaries of the XI JPL Airborne Earth Science Workshop*, 2001a.
- Plaza, A., Martínez, P., Gualtieri, J.A., Perez, R.M., "Automated identification of endmembers from hyperspectral data using mathematical morphology," *Proc. SPIE Image and Signal Processing for Remote Sensing VII*, Toulouse, France, 2001b.
- Roberts, D.A., Gardner, R., Church, R., Ustin, S., Scheer, G., Green, R.O., "Mapping Chaparral in the Santa Monica Mountains Using Multiple Endmember Spectral Mixture Models," *Remote Sensing of Environment*, vol. 65, pp. 267-279, 1998.
- Segl, K., Roessner, S., Heiden, U., "Differentiation of urban surfaces based on hyperspectral image data and a multi-technique approach," *Proceedings International Geoscience and Remote Sensing Symposium*, vol. 4 , pp. 1600-1602, 2000.
- Swayze, G., *The hydrothermal and structural history of the Cuprite Mining District, Southwestern Nevada: an integrated geological and geophysical approach*. Ph. D. Dissertation, University of Colorado, Boulder, 1997.
- Sweet, J., Granaham, J. and Sharp, M., "An Objective Standard for Hyperspectral Image Quality," *Summaries of the XII JPL Airborne Earth Science Workshop*, 2000.
- Winter, M.E., "Comparison of approaches for determining end-members in hyperspectral data," *Aerospace Conference Proceedings*, vol. 3 , pp. 305 -313, 2000.